Faculty of Physics and Astronomy

University of Heidelberg

Bachelor thesis in Physics, submitted by

Axel Donath

born in Landau/Pfalz, Germany

September 2010

Modelling Galactic γ-ray source populations

This Bachelor thesis has been carried out by Axel Donath
at the Max-Planck Institut für Kernphysik

under the supervision of Prof. Werner Hofmann

Abstract

This work deals with the modelling of galactic γ-ray source populations. This includes on the one hand the description of the spatial distribution of sources in the Galaxy and on the other hand the modelling of source properties, like spatial extension and γ-ray luminosity. The found models were investigated and compared. Using the found models simple studies were performed and it was investigated how the spiralarm structure is reflected in the resulting distributions of distance, angular extension and flux. Furthermore supernova remnants were distributed according to a Galactic model and the number of objects above interesting flux limits was determined. As result the number of 1055 sources with $\text{Flux}_\gamma > 0.1\%$ Crab Flux, 277 sources with 1% Crab flux and 26 sources with 10% Crab flux were obtained. Finally flux images were generated with different surrounding densities.

Zusammenfassung

Die vorliegende Arbeit beschäftigt sich mit der Modellierung von Populationen galaktischer γ-Quellen. Dies umfasst zum einen die Beschreibung der räumlichen Verteilung von Quellen innerhalb der Galaxie, zum anderen die Modellierung von Quelleigenschaften, wie Ausdehnung und γ-Helligkeit mit der Zeit. Die gefundene Modelle wurden untersucht und verglichen. Anhand der gefundenen Modelle wurden einfache Studien durchgeführt und dabei untersucht, wie sich die Spiralarmstruktur der Milchstraße in den resultierenden Verteilungen von Entfernung, Winkelausdehnung und Fluss widerspiegelt. Weiterhin wurden Supernovareste gemäß einem galaktischen Modell verteilt und die Anzahl der Objekte oberhalb interessanter Flussgrenzen bestimmt. Als Resultat ergaben sich eine Anzahl von 1055 Quellen mit $\text{Flux}_\gamma > 0.1\%$ Crab flux, 277 Quellen mit 1% Crab flux und 26 Quellen mit 10% Crab flux. Abschließend wurden Flussbilder bei verschiedenen Umgebungsdichten erstellt.

Contents

1 Introduction

In the last few years imaging atmospheric Cherenkov telescopes (IACTs) like HESS [1], provided a new insight to the universe by making the γ-range accessible to ground based observational astronomy. The very high energy (VHE) γ-range denotes the top end of the electromagnetic spectrum, with particle energies of $E_\gamma > 100$ GeV and can be considered as the last frontier in the field of observational astronomy.

IACTs make use of the Cherenkov effect. Cosmic γ-particles reaching the upper regions of the atmosphere interact with air particles and induce a cascade of charged secondary particles. As these particles move faster than the speed of light in air, Cherenkov light is produced, that can be observed from the ground. If this so called *particle shower* is observed from different angles, it is possible to reconstruct the direction and energy of the primary γ-particles.

Since γ-astronomy is a rather young field of research many new discoveries are expected in the near future. The main step is to build larger telescopes or arrays of telescopes, with larger light collecting areas, for example the *Cherenkov Telescope Array* (CTA)[2] project.

In order to get an idea of the number of potentially detectable objects, it is interesting to simulate the distribution and size of γ-ray sources in our home galaxy. The aim of this work is to introduce suitable models for this purpose.

1.1 The HESS Galactic plane survey

As most Galactic γ-ray sources are associated with remnants of massive stars, a concentration of sources along the Galactic plane can be observed. For this reason HESS started a systematic survey of the Galactic plane in 2004. Before 2004 only few Galactic sources were known, until now the total number has grown to ≈ 80 sources [3]. Fig.1.1 shows how HESS sees the Galactic plane between $\pm 3°$ latitude and $+60°/-85°$ longitude. During this survey HESS especially found pulsar wind nebulae as a new prominent class of Galactic γ-ray sources.

[1] http://www.mpi-hd.mpg.de/hfm/HESS/
[2] http://adsabs.harvard.edu/abs/2010arXiv1008.3703C
[3] http://tevcat.uchicago.edu/

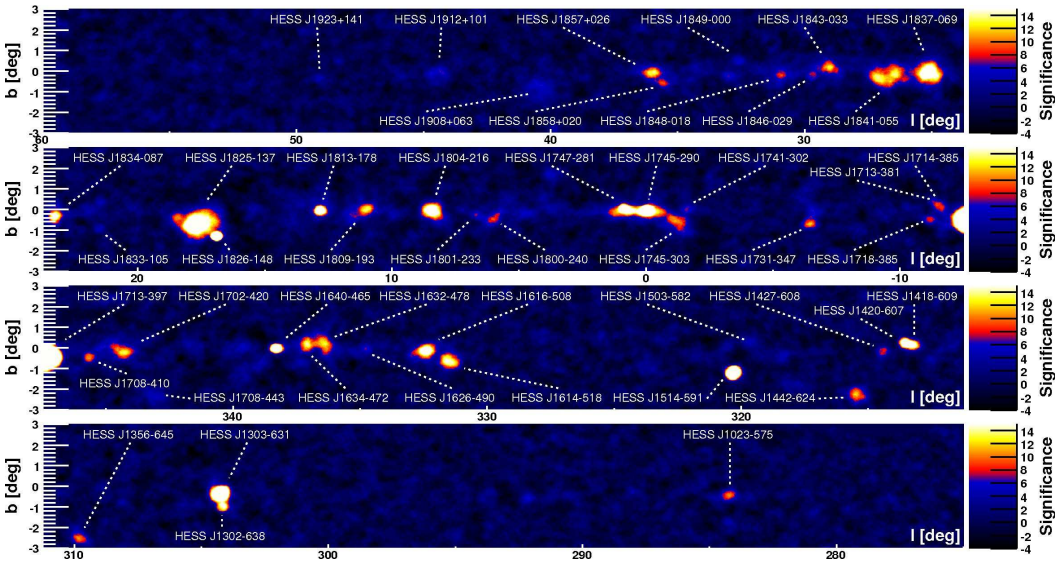

Figure 1.1: Significance map of the HESS Galactic plane survey (Chaves and for the H. E. S. S. Collaboration (2009)).

1.2 Life cycle of γ-ray sources

Most of the Galactic VHE γ-ray sources are associated with the late phases of stellar evolution. When a massive star reaches its end and has burned up all its hydrogen, the gas pressure inside decreases and the star collapses under its own graviational force, finally ending in a gigantic explosion, a so called *supernova* (SN). During the explosion, that releases energies in order of 10^{51} erg, a big part of the stellar material is ejected (at least "the outer layers") and accelerated outwards. These so called *ejecta* collide with the surrounding *interstellar medium* (ISM) and form a shock front, where the material is compressed and heated up to temperatures of 10^7-10^8 K. This interaction of stellar material with the ISM results in complex structures, that are called *supernova remnants* (SNR).

Depending on the mass of the progenitor star the SN either leaves a black hole or a neutron star. In the latter case the remaining matter of $\approx$ 1-3 $M_\odot$ is compressed into a tiny star with a radius of $\approx$ 10 km. Since angular momentum and the magnetic flux on the surface of the progenitor star are conserved, the "left over" star often rotates rapidly with a period of a few 10 ms and has a strong magnetic field with a typical value of $\approx 10^{12}$ G. As in most cases the rotation and magnetic axis are not equally alignend the neutron star emits synchrotron radiation along its magnetic axis. If the radiation cone crosses the earth, a pulsed signal, comparable to a lighthouse, can be observed. For this reason these objects are called *pulsars*.

Due to the extreme field strenghts charged particles from the surface of the pulsar are

pulled out and move along the magnetic field lines. The interaction of these particles with the surrounding medium forms a so called *pulsar wind nebula* (PWN). Fig.1.2 shows a typical shell type SNR on the left and a PWN on the right.

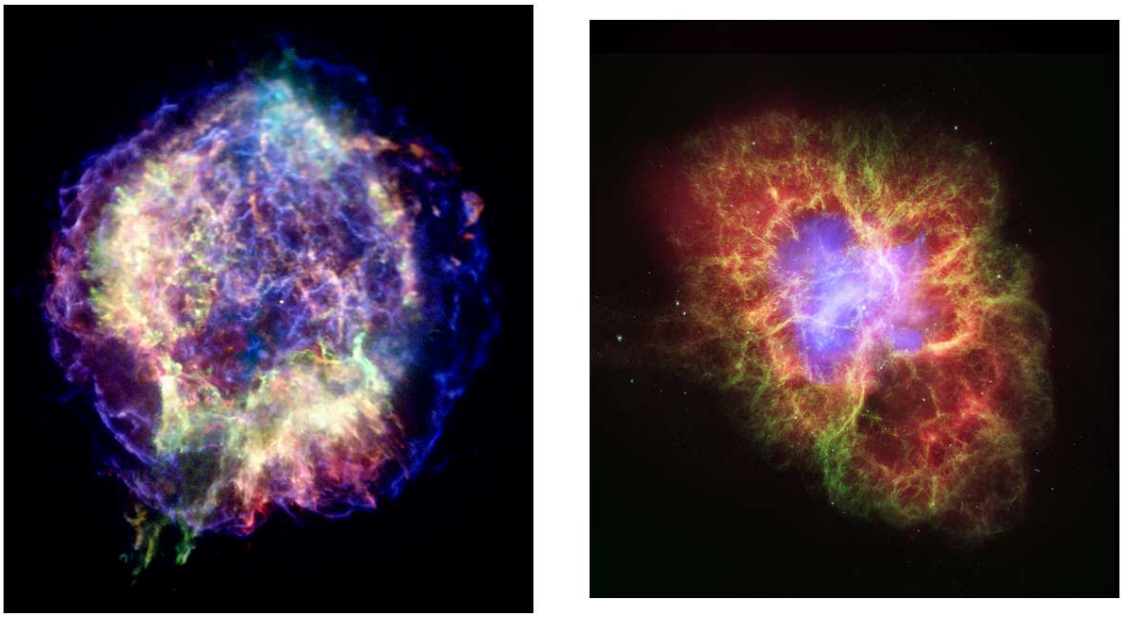

Figure 1.2: Mulitwavelength image of the SNR Cassiopeia A (left) and the Crab nebula (right). The Crab nebula is a "center filled" SNR or "Plerion".
Taken from: *http://chandra.harvard.edu/photo/category/snr.html*

1.3 Cosmic Accelerators

γ-rays have a non-thermal origin. They are mainly produced in the interaction of accelerated charged particles with ambient matter or radiation fields. Currently one assumes that mainly two processes are relevant for the production of γ-rays. At first *Inverse Compton* (IC) scattering, where target photons such as *microwave backround*, infrared or optical photons are upscattered by relativistic electrons and secondly the decay of π^0 mesons, that are produced in pp interactions. As these processes require primary particles of very high energies, one assumes the existence of *cosmic particle accelerators*. One likely mechanism is the so called *diffuse shock acceleration* in propagating shock fronts of SNRs or pulsar winds. Charged particles, such as electrons, protons or nuclei are scattered due to turbulent magnetic fields on both sides of the shock and gain energy, everytime they cross diffusively the shock.

2 Source models

In the this chapter models are presented to describe the observable properties of γ-ray sources. The task is to develop a simple description of the time evolution of the extension and luminosity of the sources. Beginning with pulsars follows the physics of SNRs and at the end of the chapter a simple model for the spatial extension of PWNe.

2.1 Pulsars

As a "central engine" pulsars affect crucially the evolution of PWNe. The model that is commonly used to describe the physical behaviour of pulsars is that of a fast rotating dipole which looses energy trough dipole radiation.

2.1.1 Spin down model

From observations of pulsed radio signals it is known that the spin frequency of a pulsar decreases with time and that the relation between the spin frequency and its time derivative can be described by a power law:

$$\dot{\Omega} = -k\Omega^n \tag{2.1}$$

n denotes the so called *braking index*. With $\Omega = 2\pi/P$ and by integrating follows the evolution of the spin period with time:

$$P(t) = P_0 \left(1 + \frac{t}{\tau_0}\right)^{\frac{1}{n-1}} \tag{2.2}$$

P_0 is the period at birth and the characteristic *spin down timescale* is defined by $\tau_0 = \frac{P_0}{(n-1)\dot{P}_0}$. The change of the period implies that the pulsar looses rotational energy with time. The rate at which rotational energy is dissipated is denoted as *spin-down luminosity* of the pulsar and given by the equation:

$$\dot{E} = \frac{d}{dt}\left(\frac{1}{2}I\Omega^2\right) = 4\pi^2 I \frac{\dot{P}}{P^3} \tag{2.3}$$

Starting its life with an initial *spin-down luminosity* of $\dot{E}_0$ the evolution is similar to 2.2:

$$\dot{E}(t) = \dot{E}_0 \left(1 + \frac{t}{\tau_0}\right)^{-\frac{n+1}{n-1}} \tag{2.4}$$

Formula 2.2 also gives an expression for the true age of the pulsar:

$$\tau = \frac{P}{(n-1)\dot{P}}\left[1 - \left(\frac{P_0}{P}\right)^{n-1}\right] \tag{2.5}$$

Since P_0 is not known for most pulsars, it is not possible to determine their true age, but assuming $P \gg P_0$ an upper limit for the age can be derived, the so called *characteristic age*:

$$\tau = \frac{P}{2\dot{P}} \tag{2.6}$$

In case of a pure dipole spin down ($n = 3$) the magnetic field on the surface of the pulsar can also be inferred from P and $\dot{P}$. The energy loss of a rotating magnetic dipole with field strength B and angular velocity Ω is known from electrodynamics [Verbunt and Heise (2003)]:

$$\dot{E} = -\frac{2B^2R^6}{3c^3}\Omega^4 \sin^2\chi \tag{2.7}$$

Where χ denotes the angle between the magnetic and the rotation axis. By setting (2.3) and (2.7) equal follows:

$$P\dot{P} = \frac{8\pi^2 R^6}{3Ic^3}\sin^2\chi B^2 \tag{2.8}$$

Assuming $\sin^2\chi \approx 1$ and with a typical moment of inertia $I_{PSR} = 10^{45} g\text{cm}^2$ and radius $R_{PSR} = 10$ km the magnetic field can be written as a convenient expression:

$$B = 3.2 \cdot 10^{19}(P\dot{P})^{1/2}G \tag{2.9}$$

According to Verbunt and Heise (2003) it seems that $\dot{E}$ does not depend on χ, because pulsars lose energy not only in form of electromagnetic radiation, but also in form of relativistic particles. As χ increases the energy loss through dipole radiation increases too, but the outflow of relativistic particles decreases. Hence for simplicity it is often assumed $\sin^2\chi \approx 1$. More complicated models include torque decay due to evolution of the magnetic field, but this effect, if at all, seems to be only relevant on timescales $\sim$ 1Myr [Verbunt and Heise (2003)] and is therefore not considered.

2.2 Supernova Remnants

Supernova remnants are structures that come along with supernovae. The stellar material that is ejected during the SN moves with supersonic speed outwards and shocks the ambient ISM. The gas is compressed and heated. In turn the shocked ambient medium pushes back on the ejecta causing a second, inwards moving shock wave, the so called *reverse shock*. The whole evolution of a SNR can be characterised in terms of several distinct stages, until it finally merges with the ISM after a time of $\approx 10^5$ yrs. As it is assumed that SNRs emit γ-radiation only in the early phases of their evolution, it is sufficient to consider the first two stages. Fig.2.1 illustrates a supernova explosion and the relevant parameters.

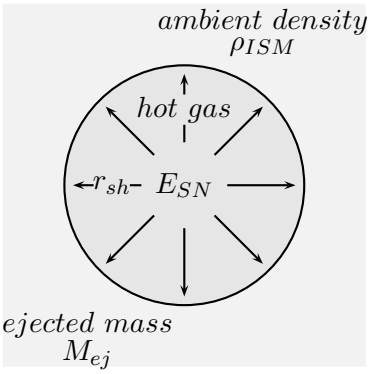

Figure 2.1: Schematic picture of a supernova explosion

2.2.1 Spatial extension

Free expansion

The first stage of the SNR's evolution is called *free expansion* or *ejecta dominated* phase. It is assumed that the ejected material is accelerated without any resistance of the surrounding medium and that the released energy E_{SN} goes completely into the kinetic energy of the ejecta:

$$E_{SN} = \frac{1}{2} M_{ej} \left(\frac{dr_{sh}}{dt} \right)^2 \tag{2.10}$$

One finds, that the radius evolves linearly with time:

$$r_{sh}(t) \approx 0.01 \text{ pc} \left(\frac{E_{SN}}{10^{51} erg} \right)^{1/2} \left(\frac{M_{ej}}{M_\odot} \right)^{-1/2} t \tag{2.11}$$

Typical velocities are in order of a few 10^4 km/s. Moving outwards the ejecta collect or "sweep up" surrounding material and their motion is decelerated. The time where the mass of the ejected material equals the mass of the swept up material marks the beginning of the next phase, the *Sedov-Taylor* phase. Assuming $\frac{4}{3}\pi r_{sh}^3 \rho_{ISM} = M_{ej}$ and formula 2.11 gives the timescale for the beginning of the *Sedov-Taylor* phase:

$$t_{ST} \approx 200 \text{ yr} \left(\frac{E_{SN}}{10^{51}\ erg} \right)^{-1/2} \left(\frac{M_{ej}}{M_\odot} \right)^{5/6} \left(\frac{\rho_{ISM}}{1 \text{ cm}^{-3}} \right)^{-1/3} \tag{2.12}$$

Sedov Taylor phase

This phase of the SNR's evolution is governed by energy conservation (in terms of thermodynamics an adiabatic expansion) and can be well described by the *Sedov solution* known from hydrodynamics. A complete description can be found in Landau and Lifschitz (2005). Essentially the radius evolves like:

$$r_{sh}(t) \propto \left(\frac{E_{SN}}{\rho_{ISM}} \right)^{1/5} t^{2/5} \tag{2.13}$$

A rather naive derivation that leads to the same result can be done as following: Assuming that the supernova is surrounded by homogeneous gas of density ρ_{ISM} and that the released energy goes into the kinetic energy of the ejected material and the swept up matter one can write:

$$E_{SN} = \frac{1}{2}(m_{ej} + m_{up}) \left(\frac{dr_{sh}}{dt}\right)^2 \tag{2.14}$$

Using $m_{ej} = m_{up} = \frac{4}{3}\pi r^3 \rho_{ISM}$ one gets for the time derivative of the radius:

$$\frac{dr_{sh}}{dt} = \left(\frac{3}{4\pi}\frac{E_{SN}}{\rho_{ISM}}\right)^{1/2} r_{sh}^{-3/2} \tag{2.15}$$

This can be integrated and after making some simple approximations the result is the same as (2.13):

$$r_{sh}(t) = \left(\frac{2}{5}\right)^{2/5} \left(\frac{3}{4\pi}\right)^{1/5} \left(\frac{E_{SN}}{\rho_{ISM}}\right)^{1/5} t^{2/5} \approx \left(\frac{E_{SN}}{\rho_{ISM}}\right)^{1/5} t^{2/5} \tag{2.16}$$

As outlined in section 1.3 the propagating shock front provides an effective mechanism for particle acceleration. Therefore the shock velocity is also an important dimension. It is given by the time derivative of r_{sh}:

$$v_{sh}(t) \propto \frac{2}{5} \left(\frac{E_{SN}}{\rho_{ISM}}\right)^{1/5} t^{-3/5} \tag{2.17}$$

Thickness of the shell

The collecting of ambient material leads to an concentration of mass at the shock front and a dense shell of *swept up* material is formed. From this shell originates most of the thermal as well as non-thermal radiation. This fact gives the SNR its characteristic appearence on the sky. As illustrated in Fig.2.2 the thickness of the shell can be estimated in a simple way.

Assuming that the shell mainly consists of shocked ambient material that is compressed from an initial density ρ_{ISM} to a density of $\rho_0 = 4\rho_{ISM}$ one can assume:

$$\frac{4}{3}\pi r_{sh}^3 \rho_{ISM} = \left(\frac{4}{3}\pi r_{sh}^3 - \frac{4}{3}\pi(r_{sh} - \Delta r)^3\right) \rho_0 \tag{2.18}$$

This yields for Δr:

$$\Delta r = r_{sh}\left(1 - \left(\frac{3}{4}\right)^{1/3}\right) \approx 0.091 r_{sh} \tag{2.19}$$

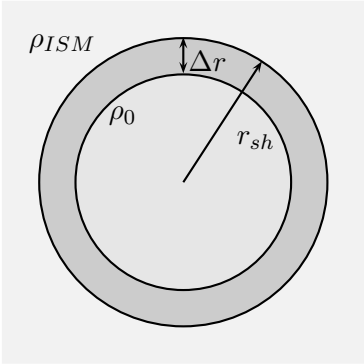

Figure 2.2: Schematic picture of the SNR shell

Literature model of Truelove and McKee (1999)

In literature exist more detailed analytical models for the evolution of an SNR. One of them is the model of Truelove and McKee (1999). In order to have an comparison, their model shall be shortly presented. It is assumed that the SNR consists of an inner core with constant density, that is surrounded by an envelope (the *ejecta*) with $\rho \propto r^{-9}$. At first the following characteristic dimensions are defined:

$$R_{ch} = M_{ej}^{1/3} \rho_{ISM}^{-1/3} \tag{2.20}$$

$$t_{ch} = E_{SN}^{-1/2} M_{ej}^{5/6} \rho_{ISM}^{-1/3} \tag{2.21}$$

Now the propagation of the shock front during the free expansion phase can be expressed as:

$$r_{sh}(t) = 1.12 R_{ch} \left(\frac{t}{t_{ch}} \right)^{2/3} \tag{2.22}$$

The transition to the Sedov Taylor Phase occurs at $t_{ST} \simeq 0.52 t_{ch}$ and then the radius evolves as:

$$r_{sh}(t) = \left[R_{SNR,ST}^{5/2} + \left(2.026 \frac{E_{SN}}{\rho_{ISM}} \right)^{1/2} (t - t_{ST}) \right]^{2/5} \tag{2.23}$$

The main advantage of this model is that it also predicts the propagation of the reverse shock, what will be important later to describe the interaction with the pulsar wind. Initially the reverse shock co-evolves with the radius of the SNR:

$$R_{RS}(t) = \frac{1}{1.19} r_{sh}(t) \tag{2.24}$$

After a time $t_{core} \simeq 0.25 t_{ch}$ the reverse shock reaches the core and then propagates as:

$$R_{RS}(t) = \left[1.49 - 0.16 \frac{t - t_{core}}{t_{ch}} - 0.46 \ln \left(\frac{t}{t_{core}} \right) \right] \frac{R_{ch}}{t_{ch}} t \tag{2.25}$$

A comparison between the simple and the Truelove model is shown in Fig.2.3. The evolution was computed for both models and for ISM densities of $n_{ISM} = 1$ cm^{-3} respectively $n_{ISM} = 0.1$ cm^{-3}. The model of Truelove& McKee predicts in general bigger SNR sizes in the Sedov Phase by the factor of ≈ 1.4. The variation of the ISM density by the factor of 10 affects the size of the SNR in both models by the factor of ≈ 1.58.

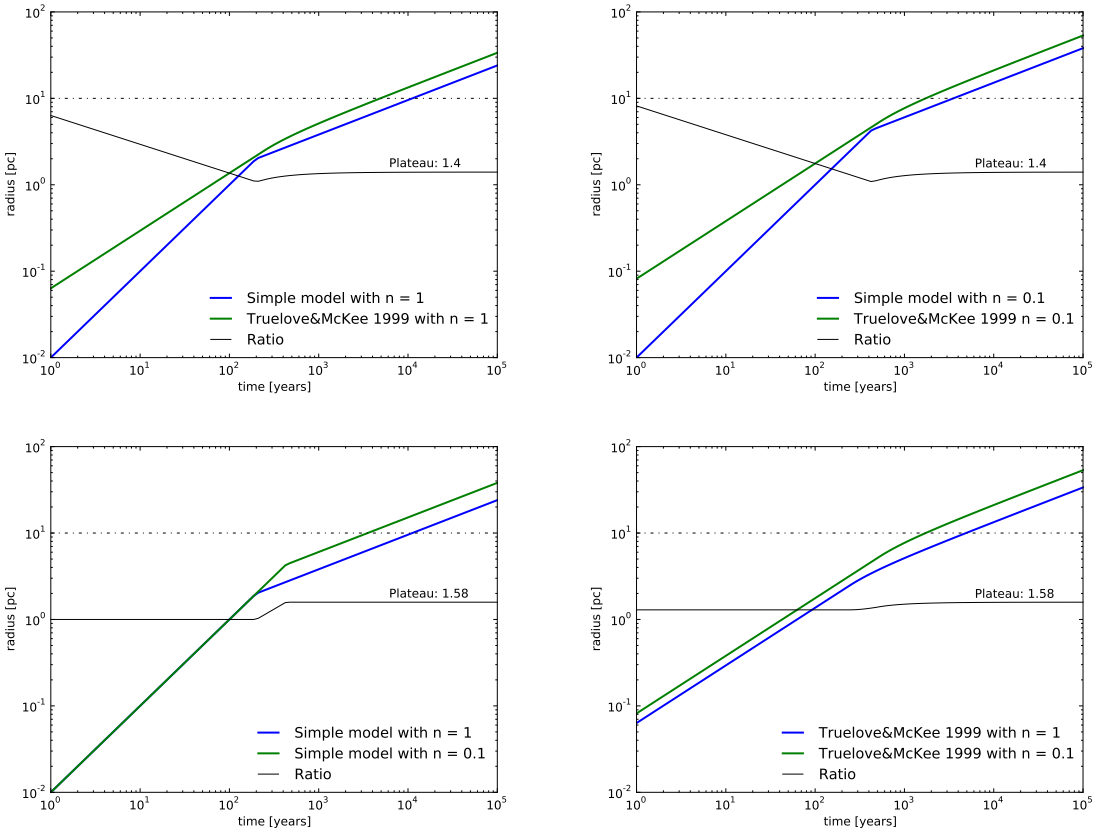

Figure 2.3: The upper plots show a comparison between the simple and the Truelove model for the ISM densities $n_{ISM} = 1$ cm^{-3} and $n_{ISM} = 0.1$ cm^{-3}. The lower plots compare the radii at different densities for each model. The other parameters are $M_{ej} = 1M_{\odot}$ and $E_{SN} = 10^{51}$ erg. The dotted line marks a radius of 10 pc, which corresponds to an angular extension of $34'$ in a distance of 1 kpc.

2.2.2 Luminosity

The description of the γ-luminosity of the SNR follows the *ad hoc* approach of Drury, Aharonian and Voelk (1994). Formula (9) in the cited paper gives an estimation for the integral flux depending on the SN energy E_{SN} and the ambient density n_{ISM}:

$$F_\gamma(>E) \approx 9{\cdot}10^{-11}\theta \left(\frac{E}{1\ TeV}\right)^{-1.1} \left(\frac{E_{SN}}{10^{51}\ erg}\right) \left(\frac{d}{1\ kpc}\right)^{-2} \left(\frac{n_{ISM}}{1\ \mathrm{cm}^{-3}}\right) cm^{-2}s^{-1} \quad (2.26)$$

θ denotes the fraction of the total supernova energy converted to cosmic rays. According to Drury, Aharonian and Voelk (1994) it is assumed that $\theta \ll 1$ during the expansion phase, because almost all of the explosion energy goes into the kinetic energy of the ejecta. Entering the Sedov phase θ should reach a roughly constant value of $\theta \approx 0.1$. SNRs emit γ-radiation only in the early phases of their evolution, because at a certain point most of the initial energy E_{SN} is radiated away via thermal radiation. The usual criterion for this is the shock temperature dropping below 10^6 K. The temperature right behind the shock is given by:

$$T_{sh} = \frac{3mv_{sh}^2}{16k} \quad (2.27)$$

Putting the shock velocity (2.17) in leads to the expression:

$$T_{sh}(t) = \frac{3m}{100k} \left(\frac{E_{SN}}{\rho_{ISM}}\right)^{2/5} t^{-6/5} \quad (2.28)$$

Inserting the criterion $T_{sh} < 10^6$ K a timescale for the end of the γ-ray emission (and for the end of the Sedov Taylor phase) can be derived:

$$t_\gamma \approx 43000\ \mathrm{yr} \left(\frac{m}{1.66 \cdot 10^{-24}\ g}\right)^{5/6} \left(\frac{E_{SN}}{10^{51}\ erg}\right)^{1/3} \left(\frac{\rho_{ISM}}{1.66 \cdot 10^{-24}\ g/cm^3}\right)^{-1/3} \quad (2.29)$$

Fig.2.4 shows the time evolution of the luminosity and the spectrum.

2.3 Pulsar Wind Nebulae

Pulsar Wind Nebulae arise when the relativistic particle wind of a pulsars is confined by the surrounding medium. Gelfand, Slane and Zhang (2009) investigated the dynamical evolution of a PWN surrounded by SN ejecta. Performing a detailed numerical simulation they were able to predict precisely the spatial as well as the spectral evolution of the PWN. Since it is not possible (and in fact not required) to perform such an accurate simulation for a few thousand model PWNe, in the following a simplified model shall be presented.

2.3.1 Spatial Extension

In general the spatial evolution of a PWN can be devided into two phases: An initial *free expansion*, where the particle plasma flows into the low dense interior of the surrounding

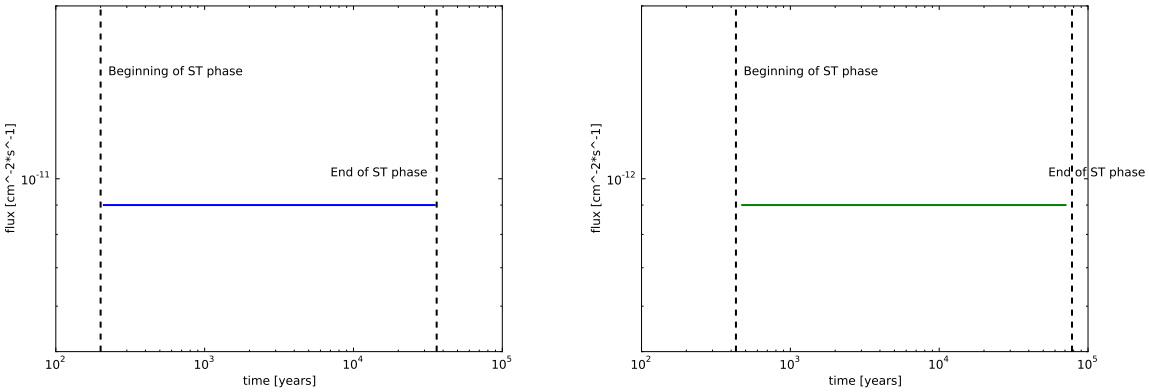

Figure 2.4: Left: Flux at 1 TeV and a distance of 1 kpc with $n_{ISM} = 1$ cm^{-3}. Right: Flux with $n_{ISM} = 1$ cm^{-3}. The corresponding γ-lifetime is significantly higher. Other parameters are: $M_{ej} = 1M_{\odot}$ and $E_{SN} = 10^{51}$ erg

SNR and a so called *reverberation phase*, that starts when the expanding PWN collides with the inwards moving reverse shock of the SNR. As the reverse shock is "stronger" the PWN is compressed, its interior pressure increases until it finally expands again. For simplicity the reverberation phase is not modelled, it is assumed, that the radius stays constant after the collision.

As shown in Gelfand, Slane and Zhang (2009) the expansion velocity is almost constant until the PWN collides with the reverse shock of the SNR. Therefore it is sufficient to use formula (8) of Gaensler and Slane (2006), that describes how the radius of the PWN evolves during the free expansion phase:

$$R_{PWN}(t) = 1.44\text{pc} \left(\frac{E_{SN}^3 \dot{E}_0^2}{M_{ej}^5} \right)^{1/10} t^{6/5} \tag{2.30}$$

It is assumed $t \ll \tau_0$ and therefore the spin down luminosity corresponds approximately to the spin down luminosity at birth $\dot{E}_0$ [compare formula (2.4)].

The time of collision is determined by $R_{PWN} = R_{RS}$. Using formula 2.24 and 2.25 for the propagation of the reverse shock this equation can be solved numerically. In order to have a comparison the radii were computed for the same set of parameters as Fig.2 in Gelfand, Slane and Zhang (2009). The left plot of Fig.2.5 shows the result.

As one can see the time of collision is $t_{coll} \approx 2000$ yrs, which is by the factor of 2 smaller than the more precise result of $t_{coll} \approx 4500$ yrs in Gelfand, Slane and Zhang (2009). This difference can be easily explained if one considers that formula 2.30 is only valid in the assumption $t \ll \tau_0$, which is not fullfilled. As a simple correction one can replace $\dot{E}_0$ in

Parameter	$\dot{E}_0$	τ_0	M_{ej}	n_{ISM}	E_{SN}
Value	10^{40} erg/s	500 yr	$8M_\odot$	0.1 #/cm^3	10^{51} erg

Table 2.1: Parameters of Gelfand, Slane and Zhang (2009)

formula 2.30 by the mean value of $\dot{E}$ between $t = 0$ and $t = t_{coll}$:

$$\dot{E}_{mean} = \frac{1}{t_{coll}} \int_0^{t_{coll}} \dot{E}_0 \left(1 + \frac{t}{\tau_0}\right)^{-2} dt = \frac{\dot{E}_0}{1 + \frac{t_c}{\tau_0}} \tag{2.31}$$

The new result is shown in the right plot of fig.2.5. The time of collision is now $t_{coll} =$ 3300 yr. As the changing of the radius of the reverse shock at this time of the evolution is rather small, the final radius of the PWN correponds quite well to the value of $\approx$ 10 pc, that was obtained by Gelfand, Slane and Zhang (2009).

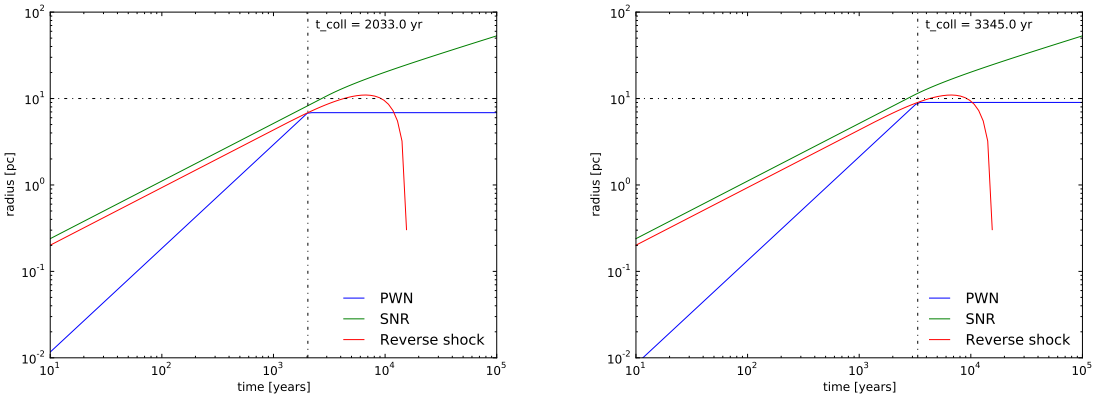

Figure 2.5: Evolution of the PWN radius, SNR radius and reverse shock. Left: Simple case. Right: Evolution with correction.

A proper model for the γ-ray luminosity of PWNe is still missing. As it is assumed that the main process of producing γ-rays in PWNe is inverse compton scattering, even a simple model should include the evolution of the electron population. This turned out to be quite complex, as not only adiabatic and synchrotron losses but also particle injection and evolution of the magnetic field have to be taken into account.

3 Population models

Beside the physical properties of γ-ray sources it is necessary to model their spatial distribution in the galaxy. Since for pulsars a reliable amount of data is available it is useful to take recent population studies, e.g Faucher-Giguère and Kaspi (2006) or Lorimer et al. (2006), as guide.

3.1 Supernova rates

A critical dimension, that determines how the sky looks in the γ-range is the total number of sources in the Galaxy respectively the rate of SN events. Recent estimations of pulsar birthrates range from 1.4 ± 0.2 per century (Lorimer et al. (2006)) to 2.8 ± 0.1 per century (Faucher-Giguère and Kaspi (2006)). Since not every SN leaves a neutron star, one can assume that the rate of SN is higher by a factor of 1.13-1.25 (Faucher-Giguère and Kaspi (2006)). Throughout this work a rate of 3 SNe per century was used. With a typical γ-lifetime of $4 \cdot 10^4$ yr this translates into a total number of $N = 1200$ objects in the Galaxy.

3.2 Interstellar medium densities

As seen in the previous chapter many properties of γ-ray sources, especially the size of SNRs and PWNe, depend crucially on the surrounding density. As a detailed model for the distribution of ISM densities in the Galaxy is not known, all studies were computed preliminaryly for densities of $n_{ISM} = 1\ cm^{-3}$ and $n_{ISM} = 0.1\ cm^{-3}$.

3.3 Spatial distribution

The models for the spatial distribution of γ-ray sources in our galaxy are mainly based on recent pulsar data. In general it is necessary to distinguish between *evolved distributions*, that are obtained from observational data to describe the current population of objects and *birth distributions*, that are used in studies to reproduce the current population of objects.

In literature this distinction is not taken to seriously, it seems that is more important to have a starting point at all. The spatial distribution is described via the surface density of the objects, commonly it is radial symmetric and just varies with the distance to the

Galactic center. The vertical distribution (height above the Galactic plane) is treated separately.

3.3.1 Radial distribution

In literature various models for the radial distribution of pulsars or other SN related objects can be found. In the following the most important will be presented.

Evolved distributions

Based on the data of the current ATNF catalog Yusifov and Küçük (2004) analyzed the radial distribution of pulsars in our galaxy. They found that the surface density could be well described by a Γ-function:

$$\rho(r) \propto \left(\frac{r}{R_\odot}\right)^a \exp\left[-b\left(\frac{r}{R_\odot}\right)\right] \tag{3.1}$$

$R_\odot$ denotes the position of the sun in the Galaxy. It was assumed that $R_\odot = 8.5$ kpc. Lorimer et al. (2006) adopted the same functional form but did not include all ATNF data and found therefore other best fit parameters. According to Case and Bhattacharya (1998) the distribution of SNRs in the galaxy can also be described by formula (3.1). In table 3.1 all values of the parameters a and b are listed.

Birth distributions

In their optimal model Faucher-Giguère and Kaspi (2006) used the the distribution of Yusifov and Küçük (2004) for the birth positions of pulsars. As this is actually an evolved distribution they proposed an alternative gaussian birth distribution (Appendix B), that led to nearly the same results:

$$p(r) \propto \exp\left[-\frac{(r-R_\mu)^2}{2\sigma^2}\right] \tag{3.2}$$

Paczynski (1990) made the assumption that the birth rate just varies exponentially with distance from the Galactic center.

$$p(r) \propto e^{-r/r_0} \tag{3.3}$$

One last possible distribution of birth positions of pulsars was proposed by Yusifov and Küçük (2004) by modifying the parameters for a and b in formula 3.1, so that the shape follows the distribution of OB stars (which are considered as progenitor stars of neutron stars) in the Galaxy.

A comparison of all distribution models is shown in fig. 3.1. The solid curves represent the current distributions, the dash-dotted lines the birth distributions. In general the

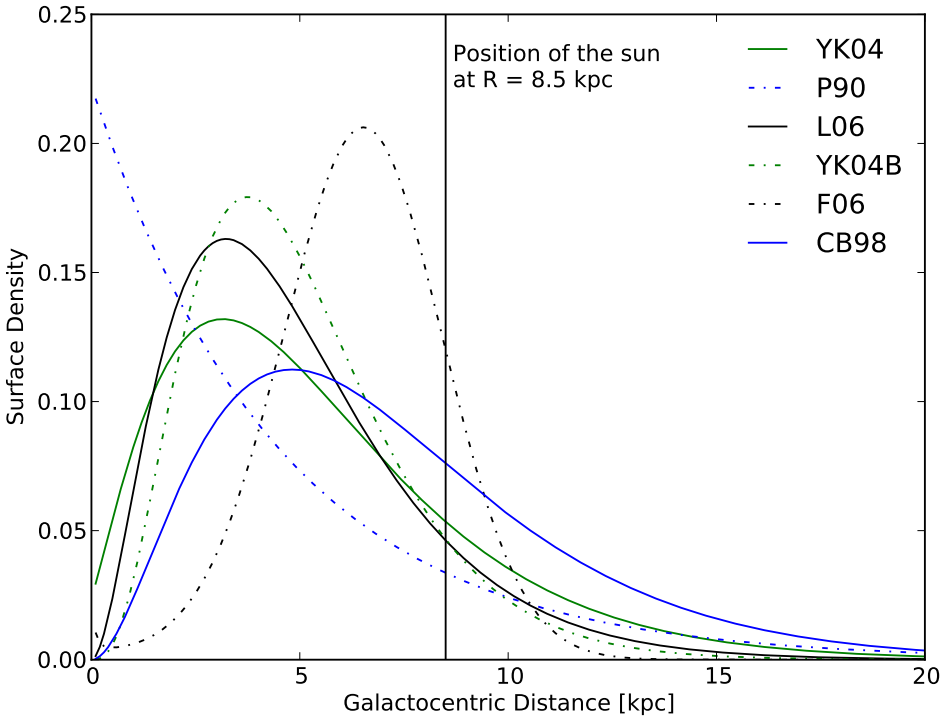

Figure 3.1: Comparison of radial distribution models. The dot dashed lines indicate birth distributions, the solid lines evolved distributions. The area under the curves is normalised to 1.

peak of the birth distributions is positioned farther from the Galactic center. This holds also for [CB98], as the distribution of SNRs can be considered as a birth distribution of pulsars. The distribution of Paczynski (1990) is an exception, because it is not based on current data.

Model	Abbreviation	Parameters	Birth	Evolved
Case and Bhattacharya (1998)	[**CB98**]	$a = 2.0$, $b = 3.53$	$(\surd)$	$\surd$
Faucher-Giguère and Kaspi (2006)	[**F06**]	$R_\mu = 7.04$ kpc, $\sigma = 1.83$ kpc	$\surd$	
Paczynski (1990)	[**P90**]	$r_0 = 4.5$ kpc	$\surd$	
Yusifov and Küçük (2004)	[**YK04**]	$a = 1.64$, $b = 4.01$		$\surd$
Yusifov and Küçük (2004)	[**YK04B**]	$a = 4.0$, $b = 6.80$	$\surd$	
Lorimer et al. (2006)	[**L06**]	$a = 1.9$, $b = 5.0$		$\surd$

Table 3.1: Parameters of the radial distribution models.

To get an impression of the "practical" differences between the introduced models the resulting distributions of Galactic longitudes and latitudes were computed. In order to reduce statistical fluctuations the distributions were computed with the hundredfold number of sources and then normalized to a number of $N = 1200$. The result is shown in Fig.3.2. The plot in the upper left corner shows the distribution of Galactic longitudes, that result from the different birth distributions. The histograms have significant differences, especially in the region of the Galactic center. The distinct peak at ≈ 7 kpc of the Gaussian birth distribution of Faucher-Giguère and Kaspi (2006) is reflected in the histogram by an increased number of sources in the region around $\pm 50°$. The longitude histogram of the current distributions shows also significant differences. As the model of Case and Bhattacharya (1998) describes the distribution of SNRs it should rather be considered as a birth distribution of neutron stars and therefore differs from the other models.

The distribution of Galactic latitudes barely depends on the choice of the radial distribution model, as it is of course mainly determined by the underlying z-distribution.

3.3.2 Z-distribution

It is commonly assumed that the current vertical distribution of pulsars follows an exponential law:

$$p(z) \propto e^{-z/z_0} \tag{3.4}$$

Based on the data of the ATNF catalog Mdzinarishvili and Melikidze (2004) investigated the distribution in the solar neighbourhood and found a scaleheight of $z_0 \approx 350$ pc. The result of Lorimer et al. (2006) was similar, they determined a scaleheight of $z_0 \approx 330$ pc.

Sartore et al. (2010) argued that for old objects the initial height distribution is not important, as they move far from their birthplaces during their lifetime. The assumption that they are all born in the Galactic plane at $z = 0$ is sufficient. As this may not hold for young objects, an initial scaleheight of $z_0 \approx 50$ pc can also be assumed. The latter value was quoted by Faucher-Giguère and Kaspi (2006) as optimal parameter to reproduce the current distribution of pulsars.

3.3.3 Spiralarm modelling

Based on observations of other spirals it is known that massive stars are mostly born in spiralarms. As it is not expected that they move far from where they were formed during their lifetime, the spiralarm structure should be considered in the distribution of birth positions of pulsars. A simple model can be taken from Faucher-Giguère and Kaspi (2006). The raw shape of each arm follows a logarithmic spiral that is defined by:

$$\Theta(r) = k\ln(r/r_0) + \Theta_0 \tag{3.5}$$

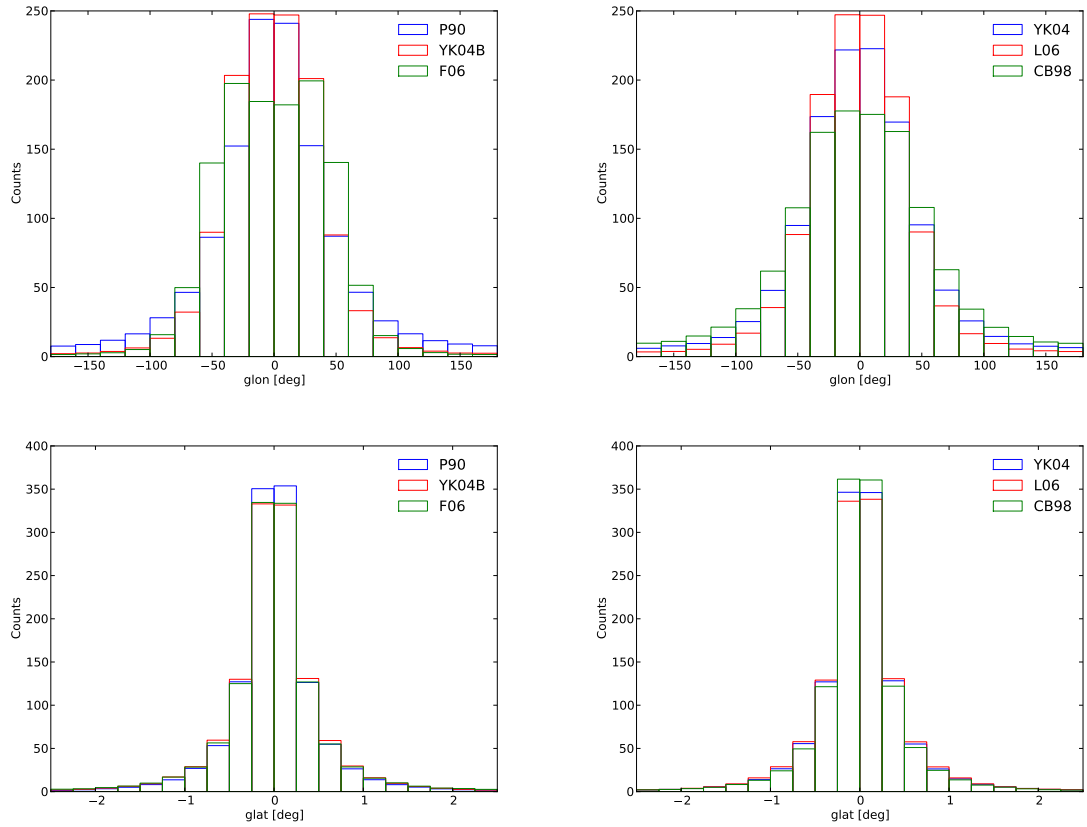

Figure 3.2: The upper plots show the distribution of Galactic longitudes, the lower plots the distribution of Galactic latitudes of the birth positions. Modelling of spiralarms was not included.

The parameters of the four known spiralarms of the milky way are shown in table 3.2. To spread the positions about the spiral centroids the x and y coordinates of each pulsar are scattered by a distance $dx = r_{corr}\cos\,\theta$ and $dy = r_{corr}\sin\,\theta$, where r_{corr} is choosen from a normal distribution centered at zero with $\sigma = 0.07r$ and θ is uniform distributed. To avoid an "unnatural" look the spiralarm structure is blurred towards the galactic center by a correction of magnitude $\theta_{corr}\exp(-0.35r/\mathrm{kpc})$, where θ_{corr} is randomly choosen between 0 and 2π. Fig.3.3 shows the result.

3.4 Initial velocities

One remarkable feature of pulsars is their proper motion. Typical space velocities range from a few 100 km/s up to 1000 km/s. One assumes that the neutron star gets a "kick" in an arbitrary direction due to an asymmetric SN or the disruption of a binary system.

Spiralarm	k [rad]	r_0 [kpc]	Θ_0 [rad]
Norma	4.25	3.48	1.57
Carina-Sagittarius	3.48	4.25	4.71
Perseus	4.89	4.90	4.09
Crux-Scutum	4.89	4.90	0.95

Table 3.2: Parameters of the four known spiralarms of the milky way.

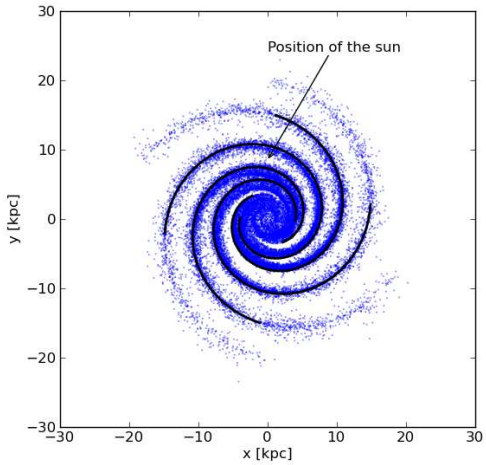

Figure 3.3: Initial positions of pulsars with the spiralarm model of Faucher-Giguère and Kaspi (2006) and radial distribution of Yusifov and Küçük (2004). The spiral centroids are drawn black.

In the following section the commonly used distributions for pulsar velocities shall be presented and compared. A detailed discussion can also be found in Faucher-Giguère and Kaspi (2006).

Two commonly used models are an exponential distribution (used by Faucher-Giguère and Kaspi (2006) in their best fit model) and a Lorentzian distribution of the components of the velocity vector. As this distributions are not isotropic (the main coordinate axes are privileged), they will not be considered.

One possible distribution for the absolute value of the space velocity was proposed by Paczynski (1990):

$$p(v) = \frac{4}{\pi v_0 \left(1 + \left(\frac{v}{v_0}\right)^2\right)^2} \tag{3.6}$$

Model	Abbreviation	Parameters
Paczynski (1990)	[**F06P**]	$v_0 = 560$ km/s
Faucher-Giguère (2006) Maxwellian	[**H05**]	$\sigma = 290$ km/s
Faucher-Giguère (2006) Bimodal	[**F06B**]	$w = 0.9$, $\sigma_1 = 160$ km/s, $\sigma_2 = 780$ km/s

Table 3.3: Parameters of the velocity distribution models

The corresponding parameters are listed in table 3.3. Like the radial distribution the velocity distribution of Paczynski (1990) is an exception, as it favors low velocities and is based on old data. Therfore it should be considered just for completeness. Another commonly used model is the Maxwellian distribution, that results from a component-wise Gaussian distribution:

$$p(v) = \sqrt{\frac{2}{\pi}} \frac{v^2}{\sigma^3} \exp\left(-\frac{v^2}{2\sigma^2}\right) \tag{3.7}$$

In order to take two "kick mechanisms" into account a Maxwellian distribution with two means is also possible:

$$p(v) = \sqrt{\frac{2}{\pi}} v^2 \left[\frac{w}{\sigma_1^3} \exp\left(-\frac{v^2}{2\sigma_1^2}\right) + \frac{1-w}{\sigma_2^3} \exp\left(-\frac{v^2}{2\sigma_2^2}\right)\right] \tag{3.8}$$

To estimate the difference between the several models, again the resulting distributions of Galactic longitudes and latitudes were computed. Fig.3.4 shows the comparison. As one can see the final distribution of Galactic longitudes and latitudes barely depends on the choice of the initial velocity model. This is conform to the result of Faucher-Giguère and Kaspi (2006), that found no significant differences between the distributions of initial velocities, even for old objects.

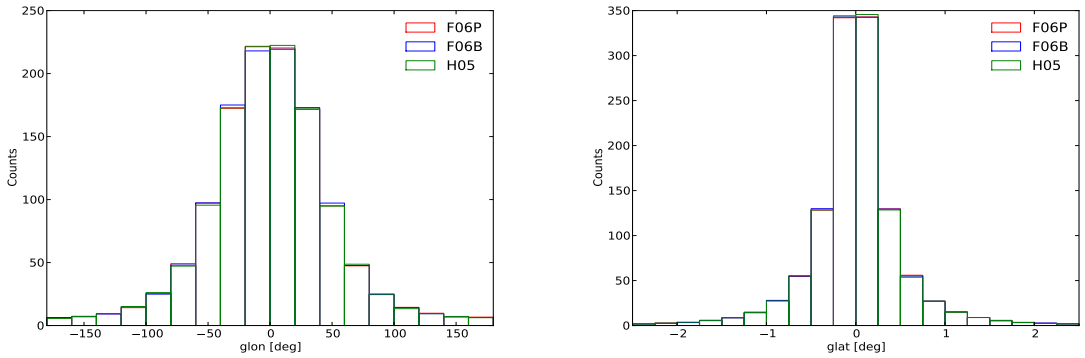

Figure 3.4: Distribution of the Galactic longitudes and latitudes resulting from different velocity models. As maximal age was assumed $age_{max} = 4e4$ yr

3.5 Timescales of pulsar motion

3.5.1 Galactic potential

Recent population studies all consider the influence of the Galactic potential on the motion of pulsars. In the most extrem case pulsars are caused to oscillate through the galactic plane. This effect can be used to estimate a timescale and to find out if this influence is relevant four young objects:

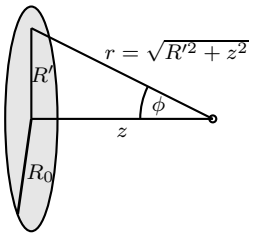

Figure 3.5: Gravitional force acting on a pulsar perpendicular to the Galactic plane

Assuming a surface mass density ρ_0 and a radius R_0 of the galaxy, the infintesimal force projected in z-direction is, as illustated in figure 3.5:

$$dF(z) = \gamma \frac{m\rho_0}{r^2} \cos\,\phi \cdot dA = \gamma m \rho_0 \frac{R'z}{(z^2 + R'^2)^{3/2}} \cdot dR' d\varphi \tag{3.9}$$

The total force is obtained via integration:

$$\begin{aligned} F(z) = \int dF &= 2\pi\gamma m\rho_0 z \int_0^R \frac{R'}{(z^2 + R'^2)^{3/2}} dR' = 2\pi\gamma m\rho_0 z \left[-\frac{1}{\sqrt{z^2 + R'^2}} \right]_0^R \\ &= 2\pi\gamma m\rho_0 \left[-\frac{z}{R_0\sqrt{1 + (z/R_0)^2}} + 1 \right] \end{aligned} \tag{3.10}$$

The constant term in the brackets can be interpreted as a shift of the rest position and does not matter. Assuming $z \ll R_0$ quadratic terms can be neglected:

$$\frac{z}{R_0\sqrt{1 + (z/R_0)^2}} \approx \frac{z}{R_0} \tag{3.11}$$

The result is analog to Hooke's law:

$$F(z) = -kz \qquad \text{with } k = \frac{2\pi\gamma m\rho_0}{R_0} \tag{3.12}$$

With a Galactic radius of $R_0 = 15$ kpc and total mass $M_0 = 5.6 \cdot 10^{11} M_\odot$ the oscillation period is approximatly:

$$T_{PSR} = 2\pi\sqrt{\frac{m}{k}} \approx 160 \text{ Myr} \tag{3.13}$$

The Galactic potential affects the motion only on timescales that are very large compared to the age of the considered sources. Therefore it should be sufficient to tread their motion as linear. A complex modelling of the Galactic gravitational potential and a time-consuming computation of orbits is not required.

3.5.2 Motion in the sky

To illustrate that the motion on short timescales is still relevant, fig. 3.6 shows how far young pulsars can travel during their lifetime and thereby change significantly their position in the sky.

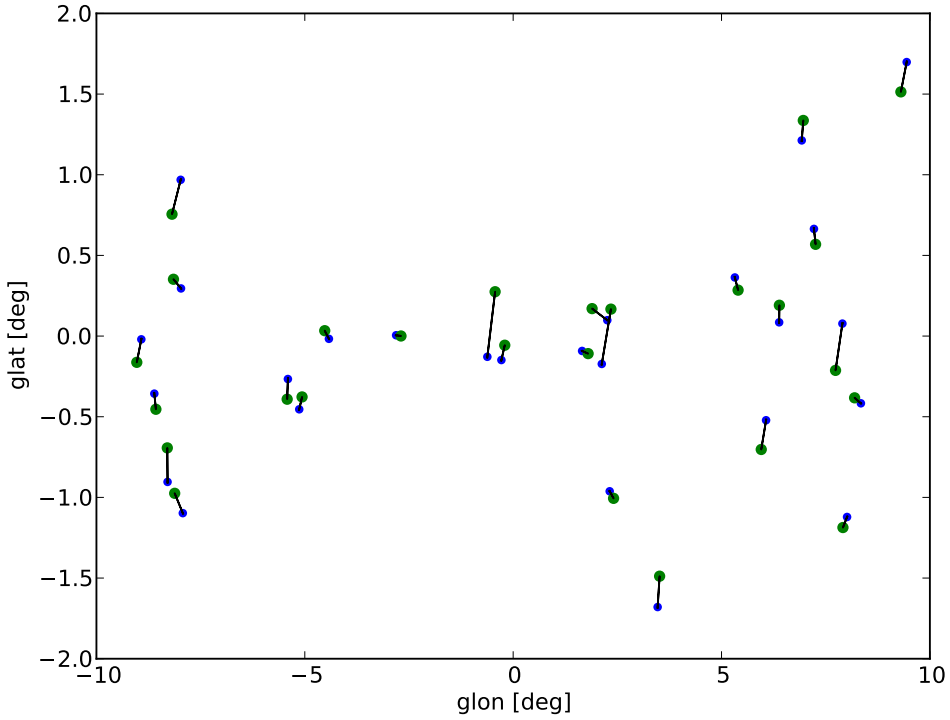

Figure 3.6: Random sample of pulsars which moved more than 0.1° since birth and are younger than $4 \cdot 10^4$ yr. Birth positions are green marked, current positions blue

4 Catalog studies

To characterise a whole population of Galactic sources one makes use of statistics. A possible approach is to investigate the distribution of object properties such as position, angular extension or flux. In this chapter some preliminary results shall be presented, in how far different spatial arrangements are reflected in such diagrams. Starting with a basic study of homogeneous distributed sources with definite properties, follows the investigation of a more realistic case, that includes the afore presented spatial distribution models.

4.1 Homogeneous distributions

As a first study a given number of sources, with definite properties (constant luminosity = 1 and extension = 1) were homogeneously distributed in a certain volume and the resulting Log N diagrams of angular extension Θ, flux s and distance R were computed. Several cases were considered:

- **One-dimensional case**: Distribution of objects along a line with a linear density ρ_{1D}. This corresponds to the distribution of sources along a spiral arm.
- **Two-dimensional case**: Distribution of sources in a plane with surface density ρ_{2D}. This corresponds to the distribution of sources in a galactic disk.
- **Three-dimensional case**: Distribution of sources in a volume with density ρ_{3D}. This corresponds to the distribution of sources in a bulge.

4.1.1 Analytical derivation

The characteristic slopes of the resulting histograms can be derived analytically. This shall be shown for the one dimensional case:

Distance R

Assuming a linear density ρ_{1D} and a binsize of ΔR of the histogram, we get for the total number of sources in dependence of the distance R:

$$N(R) = \int_{R}^{R+\Delta R} \rho_{1D} dr = 2\rho_{1D}\Delta R \tag{4.1}$$

This has to be transformed to $y = \lg R$, with $\Delta R = \ln 10 R \Delta y$:

$$N(y) = 2\rho_{1D} \ln 10 R \Delta y \tag{4.2}$$

One finally obtains for $\lg N(\lg R)$:

$$\lg N(\lg R) = \lg \left(2\rho_{1D}\Delta(\lg R)\ln 10\right) + \lg R \tag{4.3}$$

One can see that the expected slope of the Log N - Log R diagram is $m = 1$.

Angular extension Θ

The distribution of the angular extension Θ can be derived if one uses that $\Theta = 1/R$. Starting from equation 4.1 one can replace $\Delta R = R^2 \Delta\Theta$. Transforming to $\lg\Theta$ yields:

$$\lg N(\lg \Theta) = \lg \left(2\rho_{1D} \ln 10 \Delta(\lg \Theta)\right) - \lg \Theta \tag{4.4}$$

In this case the expected slope in the Log N - Log Θ diagram is $m = -1$.

Flux s

The distribution of the flux is obtained in the same way. It holds that $s = 1/4\pi R^2$. Again from equation 4.1 one replaces $\Delta R = 2\pi R^3 \Delta s$. After transforming to $\lg s$ one obtains:

$$\lg N(\lg s) = \lg \left(\frac{1}{\sqrt{4\pi}} \rho_{1D} \ln 10 \Delta(\lg s)\right) - \frac{1}{2}\lg s \tag{4.5}$$

The expected slope for the Log N - Log s diagram is $m = -1/2$. Following the same procedure the slopes for the two- and three-dimensional case can also be determined.

4.1.2 Simulation

The characteristic slopes were also determined via simulation. A total number of $N = 1200$ objects was randomly distributed on a line of length 20 kpc respectively in a square and a cube of the same side and edge length. The slope of the distributions was determined by fitting a straight line, that is also plotted. The resulting histograms of d, Θ and s are shown in fig. 4.1. The artefacts at the top end of the 2-D and 3-D distribution steem from the fact that the sources were not distributed spherically symmetric. Therefore the number of sources at high distances (i.e. the objects that are placed in the "corners") decreases. Table 4.1 summarises all obtained values.

Distribution	Distance d	Extension Θ	Flux s
Theorical values:			
1-D	1	-1	$-1/2$
2-D	2	-2	-1
3-D	3	-3	$-3/2$
Simulated values:			
1-D	0.99	-0.99	-0.49
2-D	2.02	-2.02	-1.01
3-D	2.93	-2.89	-1.45

Table 4.1: Expected slopes of the Log N Log d, θ, s distributions and the values that were obtained from the simulations.

4.2 Galactic distribution and spiral arm structure

Now a more realistic scenario shall be considered, where SNRs are distributed in a model Galaxy. Especially shall be investigated how the spiral arm structure is reflected in the resulting Log d, Θ and s distributions.

4.2.1 Method

In order to obtain the right random numbers for the birth positions the probability density function (PDF) has to be derived from the given surface density distribution in chapter 3. Probability density $p(R)$ and surface density $\rho(R)$ are related through:

$$p(R)dR = \frac{R\rho(R)dR}{\int_0^\infty R\rho(R)dR} \tag{4.6}$$

The random values for the initial positions are than drawn from the PDF using the inversion method. All other relevant properties of the sources are obtained according to the following procedure:

- Random initial positions and velocities are drawn
- Age is drawn from a uniform distribution and the final position is computed
- Surrounding parameters E_{SN} and ρ_{ISM} are set
- Properties of the SNRs are computed
- Observed properties are added (Flux s, angular extension Θ, ...)

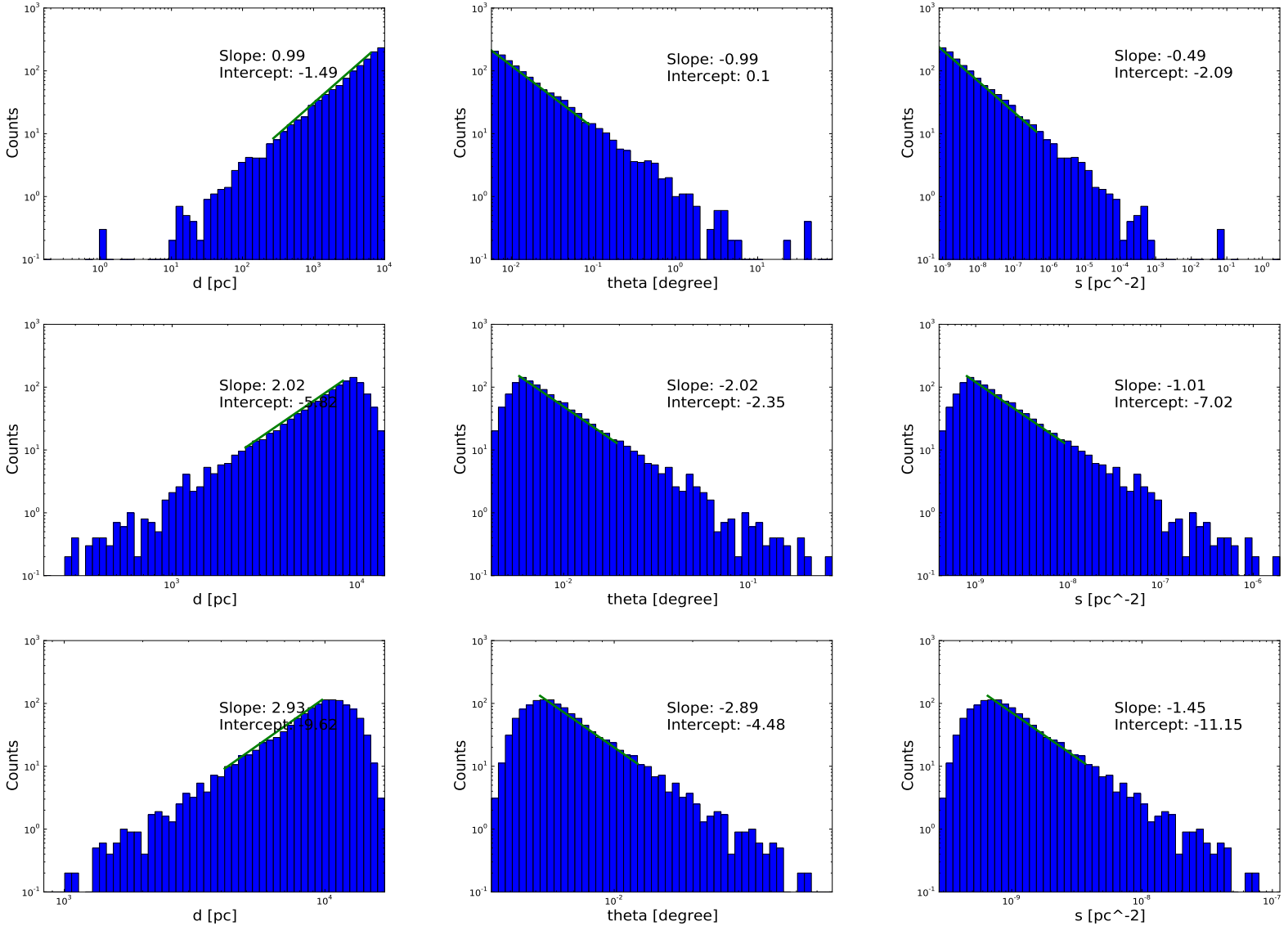

Figure 4.1: One-(first row), two-(second row) and three-(third row) dimensional homogeneous distribution of objects and resulting Log N histograms of distance d, angular extension Θ and flux s.

4.2.2 Preliminary results

The SNRs were distributed assuming the radial model of Yusifov and Küçük (2004) and the Maxwellian velocity distribution. The spiral arm structure was not taken into account. All SNRs had the same constant luminosity, their spatial extension was computed according to the simple model. The left column of fig.4.2 shows the resulting distributions. Again a straight line was fitted to determine the characteristic slopes. Comparing with the homogeneous distributions of the previous section, the slopes correspond quite well to the two-dimensional case. The obtained values are listed in table 4.2.

As next step the same parameters as before were assumed, but the spiral arm structure was taken into account. The right column of fig.4.2 shows the resulting histograms of log d, Θ and s. The obtained slopes are again listed in table 4.2.

	Distance d	Extension Θ	Flux s
Without spiralarms	1.91	-1.88	-0.93
With spiralarms	1.62	-1.52	-0.74

Table 4.2: Slopes of the Log N - distributions with and without spiralarm structure.

As one can see the slopes of the distributions that include the spiral arm structure are shifted significantly towards the slopes of the one-dimensional case. A second effect is that the number of sources at small distances (i.e. in the neighbourhood of the sun) decreases causing a "knee" in the slope.

Based on the same distribution model some final predictions shall be made. Table 4.3 summarises the number of SNRs listed by flux limits and the median values of the corresponding longitudes, latitudes and angular extension. For the Crab flux was used $F_\gamma(> 1TeV) = 1.75 \cdot 10^{-11}\mathrm{cm}^{-2}s^{-1}$ (Aharonian et al. (2004)).

Flux limit [Crab Flux]	Number of sources	Median $\lvert l\rvert$ [°]	Median $\lvert b\rvert$ [°]	Median Θ [°]
> 1	0	-	-	-
> 0.1	26	47.3	1.2	0.38
> 0.01	277	39.3	0.4	0.14
> 0.001	1055	28.1	0.2	0.06

Table 4.3: Predicted number of sources and median values of l, b and Θ listed by flux limits.

In the HESS regime ($\mathrm{Flux}_\gamma > 1\%$ Crab Flux) a total number of 277 potentially detectable sources is predicted. Assuming a flux limit of $\mathrm{Flux}_\gamma > 0.1\%$ Crab Flux, as it is planned for CTA, the number of sources approximatly quadruples.

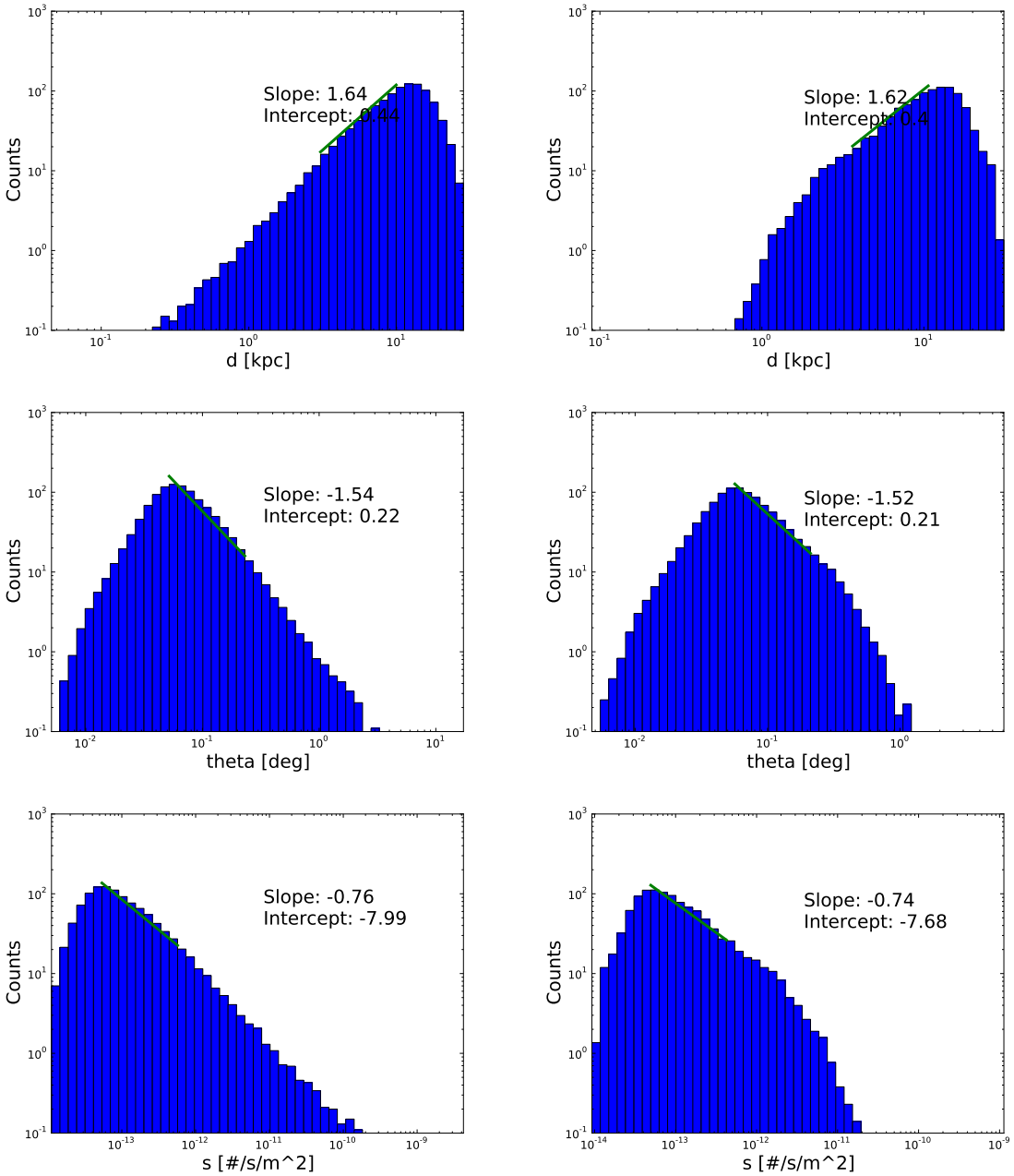

Figure 4.2: Log N - Log d, Θ, s diagrams of the Galaxy populated with $N = 1200$ SNRs. The used parameters are: $n_{ISM} = 1$ cm^{-3} , $E_{SN} = 10^{51}$ erg and $M_{ej} = 1M_{\odot}$. The left column shows the distribution with taking the spiralarm structure into account, the right column shows the distribution without spiralarm structure.

5 Flux Images

As final step flux maps shall be computed from the generated catalogs, to give an impression how a given distribution of SNRs appears in the sky.

5.1 Morphology model for SNRs

As it is assumed that the γ-ray emission is mainly limited to the dense region at the shock front, the SNR is treated as a shell of constant luminosity with given inner radius R_{in} and outer radius R_{out}. As no simpler model for the thickness of the shell exists, the estimation that was derived in chapter 2 is used to determine the inner radius. It holds that $R_{in} = 0.91 R_{out}$. The resulting distribution of the flux can be obtained via line of sight integration and is described by:

$$L_\gamma(r) = L_0 \cdot \begin{cases} \sqrt{R_{out}^2 - r^2} - \sqrt{R_{in}^2 - r^2} & \text{for} \quad r < R_{in} \\ \sqrt{R_{out}^2 - r^2} & \text{for} \quad R_{in} < r < R_{out} \\ 0 & \text{for} \quad r > R_{out} \end{cases} \tag{5.1}$$

L_0 is choosen such, that the total integrated luminosity is the corresponding total flux L_γ steeming from the source. Fig. 5.1 shows the radial profile normalised to $L_\gamma = 1$ and the corresponding 2D image.

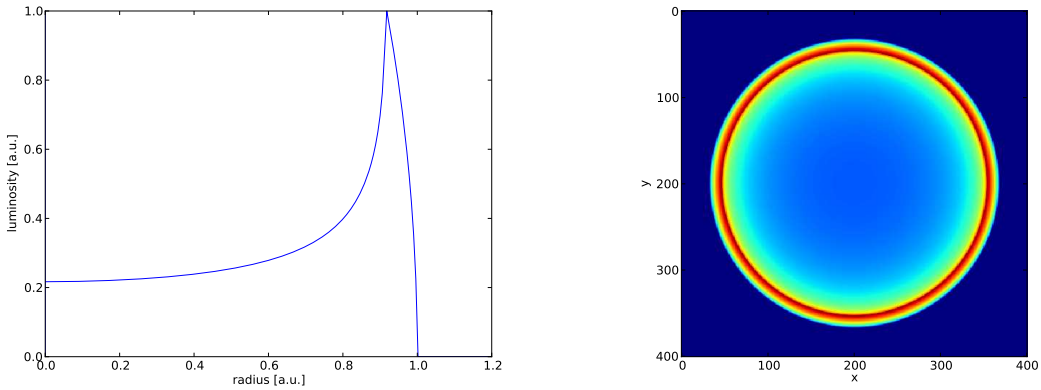

Figure 5.1: Radial profile and 400x400 Pixel image of the shell model

5.2 Images

The following image was computed assuming a supernova rate of 3 per century and a surrounding density of $n_{ISM} = 0.1$ cm^{-3}. It shows the region of the Galactic center with the field of view: ±50° l and ±20° b:

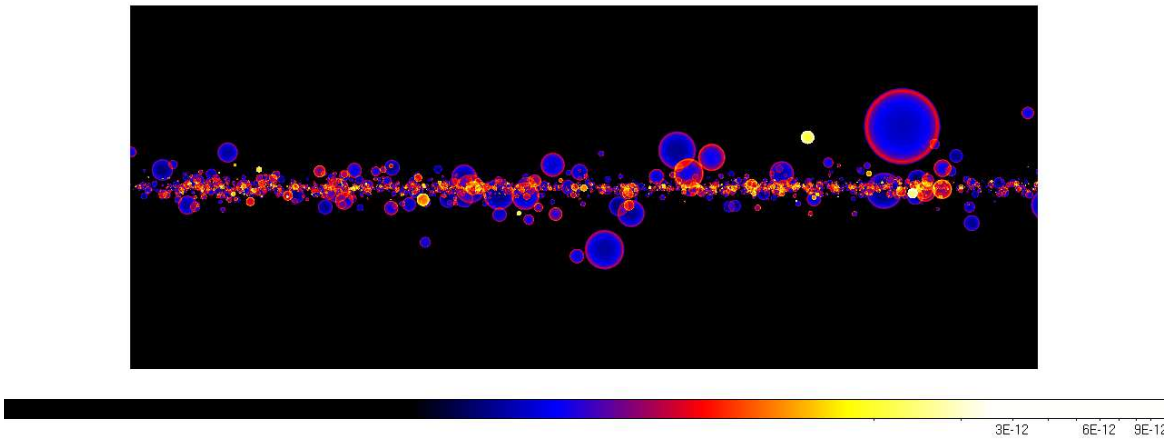

Figure 5.2: The galaxy populated with SNRs at $n_{ISM} = 0.1$.

In the following image the field of view was changed to ±5° l and ±2° b to obtain a closer view on the Galactic center:

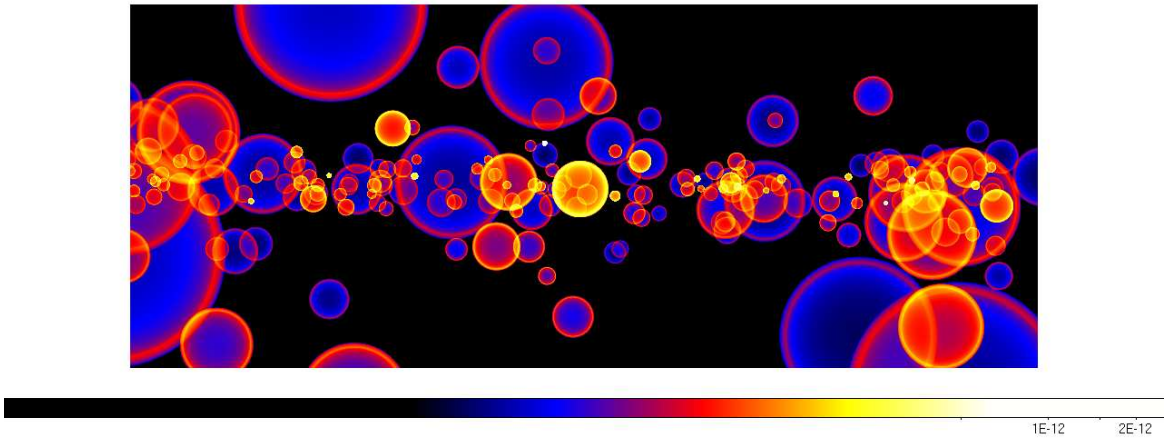

Figure 5.3: The galaxy populated with SNRs at $n_{ISM} = 0.1$

Assuming the same supernova rate as above but with a ISM density of $n_{ISM} = 1$ the regions look as following: Closer view on the Galactic center:

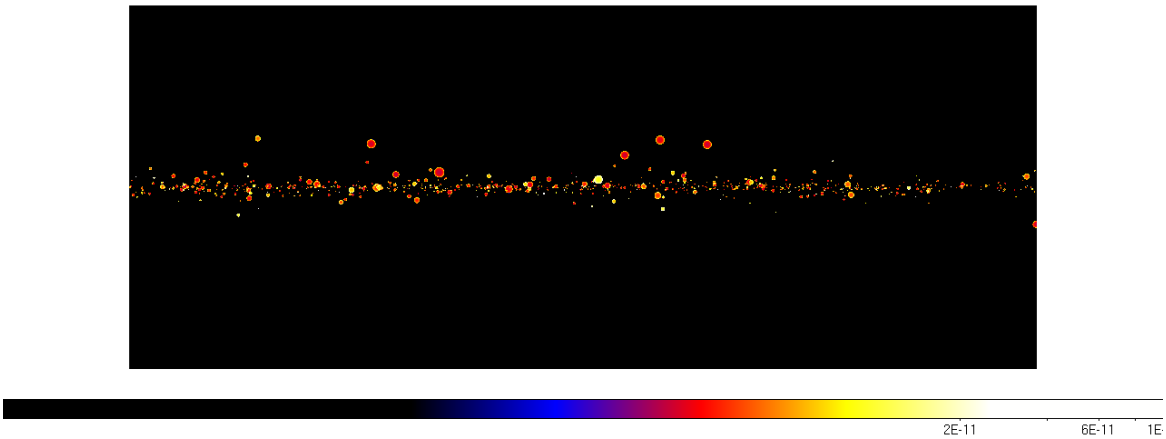

Figure 5.4: The galaxy populated with SNRs at $n_{ISM} = 1$

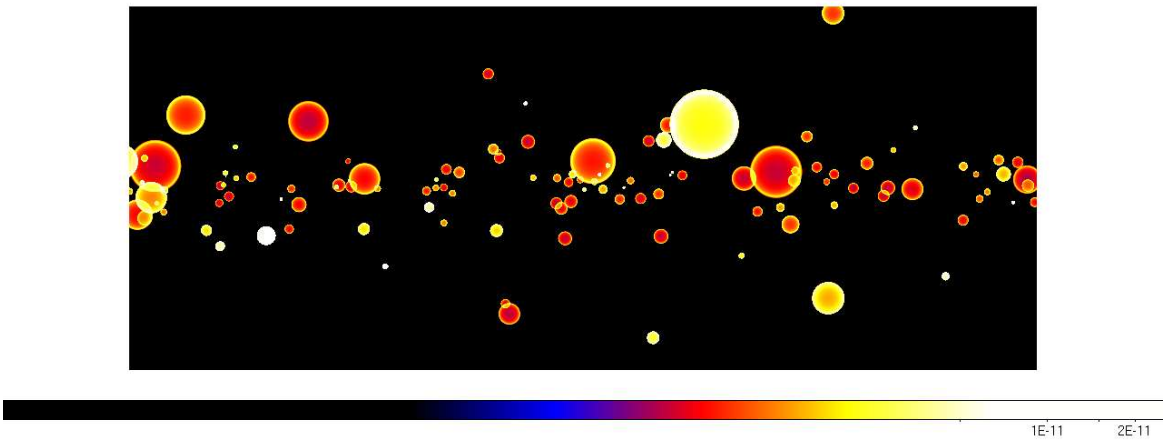

Figure 5.5: The galaxy populated with SNRs at $n_{ISM} = 1$ Galactic center

Comparing the two images by eye, one can notice that with an ISM density of $n_{ISM} = 0.1\ \mathrm{cm}^{-3}$ the SNRs can reach bigger sizes, but the luminosity is fainter. A further observation is that the total number of sources is higher in the case with $n_{ISM} = 0.1\ \mathrm{cm}^{-3}$. This can be explained if one considers that a smaller ISM density increases the γ-lifetime of the SNRs.

6 Summary and Outlook

In this work were presented simple models to describe the spatial distribution, and observable properties of γ-ray sources in our home Galaxy. At first two models for the radius of SNRs were compared and it turned out that they predict different radii in the Sedov phase by a factor of ≈ 1.4. The following model for the spatial evolution of PWNe proved to be imprecise, as the time of collision with the reverse shock of the SNR differed by a factor of ≈ 2 from the literature result. This could be corrected with a simple consideration, so that the correct value was approximately obtained.

It was shown further that the choice of the initial velocity model is of minor importance for the final spatial distribution of sources, whereas the radial distribution models had significant differences in the resulting longitude histograms. By simple analytical calculations an estimation for the thickness of a SNR's shell was derived and the timescale of the influence of the Galactic potential on the motion of sources was determined. Afterwards followed a qualitative investigation of the spiral arm structure's influence on Log N - Log d, Θ s diagrams.

The distribution of SNRs according to a Galactic arrangement predicted a number of 277 sources with a flux of $Flux_\gamma > 1\%$ Crab Flux and 1055 sources with $Flux_\gamma > 0.1\%$ Crab Flux. Finally flux images were computed, as a basis for future qualitative studies and "promotion" images.

The main step to complete the modelling of Galactic γ-ray sources is to develop a model for the luminosity of PWNe, that can be included in future studies. A comparison of the obtained results with recent HESS data is also still owing.

Bibliography

[1] F. Aharonian et al. "The Crab Nebula and Pulsar between 500 GeV and 80 TeV: Observations with the HEGRA Stereoscopic Air Cerenkov Telescopes". In: *apj* 614 (Oct. 2004), pp. 897–913. DOI: 10.1086/423931. eprint: arXiv:astro-ph/0407118.

[2] G. L. Case and D. Bhattacharya. "A New Sigma -D Relation and Its Application to the Galactic Supernova Remnant Distribution". In: *apj* 504 (Sept. 1998), pp. 761–+. DOI: 10.1086/306089. eprint: arXiv:astro-ph/9807162.

[3] R. C. G. Chaves and for the H. E. S. S. Collaboration. "Extending the H.E.S.S. Galactic Plane Survey". In: *ArXiv e-prints* (July 2009). eprint: 0907.0768.

[4] L. O. Drury, F. A. Aharonian and H. J. Voelk. "The gamma-ray visibility of supernova remnants. A test of cosmic ray origin". In: *aap* 287 (July 1994), pp. 959–971. eprint: arXiv:astro-ph/9305037.

[5] C.-A. Faucher-Giguère and V. M. Kaspi. "Birth and Evolution of Isolated Radio Pulsars". In: *apj* 643 (May 2006), pp. 332–355. DOI: 10.1086/501516. eprint: arXiv:astro-ph/0512585.

[6] B. M. Gaensler and P. O. Slane. "The Evolution and Structure of Pulsar Wind Nebulae". In: *araa* 44 (Sept. 2006), pp. 17–47. DOI: 10.1146/annurev.astro.44.051905.092528. eprint: arXiv:astro-ph/0601081.

[7] J. D. Gelfand, P. O. Slane and W. Zhang. "A Dynamical Model for the Evolution of a Pulsar Wind Nebula Inside a Nonradiative Supernova Remnant". In: *apj* 703 (Oct. 2009), pp. 2051–2067. DOI: 10.1088/0004-637X/703/2/2051. eprint: 0904.4053.

[8] L.D. Landau and E.M. Lifschitz. *Lehrbuch der Theoretischen Physik, Band 6, Hydrodynamik*. 2005.

[9] D. R. Lorimer et al. "The Parkes Multibeam Pulsar Survey - VI. Discovery and timing of 142 pulsars and a Galactic population analysis". In: *mnras* 372 (Oct. 2006), pp. 777–800. DOI: 10.1111/j.1365-2966.2006.10887.x. eprint: arXiv:astro-ph/0607640.

[10] T. G. Mdzinarishvili and G. I. Melikidze. "On the z-distribution of pulsars". In: *aap* 425 (Oct. 2004), pp. 1009–1012. DOI: 10.1051/0004-6361:20034410.

[11] B. Paczynski. "A test of the galactic origin of gamma-ray bursts". In: *apj* 348 (Jan. 1990), pp. 485–494. DOI: 10.1086/168257.

[12] N. Sartore et al. "Galactic neutron stars. I. Space and velocity distributions in the disk and in the halo". In: *aap* 510 (Feb. 2010), A23+. DOI: 10.1051/0004-6361/200912222. eprint: 0908.3182.

[13] J. K. Truelove and C. F. McKee. "Evolution of Nonradiative Supernova Remnants". In: *apjs* 120 (Feb. 1999), pp. 299–326. DOI: 10.1086/313176.

[14] F. Verbunt and J. Heise. *Neutron Stars, 3rd year astronomy course, Astronomical Institute Utrecht*. 2003.

[15] I. Yusifov and I. Küçük. "Revisiting the radial distribution of pulsars in the Galaxy". In: *aap* 422 (Aug. 2004), pp. 545–553. DOI: 10.1051/0004-6361:20040152. eprint: arXiv:astro-ph/0405559.

Danksagung

Mein aufrichtiger Dank gilt:

Professor Werner Hofmann für die Möglichkeit in seiner Arbeitsgruppe erste Forschungerfahrung sammeln zu dürfen.

Christoph Deil für die zuverlässige Betreung, das Beantworten von vielen "kurzen Fragen" zu PYTHON, das sich manchmal als hinterlistige Schlange erwies, das "mal 'ne Minute haben", das Korrekturlesen und die nützlichen Hinweise kurz vor Abgabe der Arbeit.

Joachim Hahn für die Hilfe bei den Pulsar Wind Nebeln, die es dann doch nicht mehr in die Arbeit geschafft haben...und für das aufmunternde "Na, du Streber":-)

Meinen Eltern und meiner Schwester, für die offenen Ohren...

Erklärung:

Hiermit versichere ich, dass ich diese Arbeit selbständig verfasst und keine anderen als die angegebenen Quellen und Hilfsmittel benutzt habe.

Heidelberg, den ....
(*Unterschrift*)